JGR Space Physics

RESEARCH ARTICLE
10.1029/2020JA028968

GPS Scintillations and TEC Variations in Association With a Polar Cap Arc

Yong Wang[1,2], Zheng Cao[1], Zan-Yang Xing[1], Qing-He Zhang[1], P. T. Jayachandran[2], K. Oksavik[3,4], Nanan Balan[1], and K. Shiokawa[5]

[1]Shandong Provincial Key Laboratory of Optical Astronomy and Solar-Terrestrial Environment, School of Space Science and Physics, Institute of Space Sciences, Shandong University, Weihai, China, [2]Physics Department, University of New Brunswick, Fredericton, NB, Canada, [3]Birkeland Centre for Space Science, Department of Physics and Technology, University of Bergen, Bergen, Norway, [4]Department of Arctic Geophysics, University Centre in Svalbard, Longyearbyen, Norway, [5]Institute for Space-Earth Environmental Research, Nagoya University, Nagoya, Japan

Key Points:

- We report a polar cap arc producing clear amplitude and phase scintillations on GPS L-band signals with large total electron content (TEC) enhancements
- The polar cap arc moved at a horizontal speed of ~700 m/s, as revealed by simultaneous ground-based all-sky 557.7 and 630.0 nm images
- Both scintillation bursts are likely related to the significant TEC enhancements and flow shears associated with the polar cap arc

Correspondence to:
Z.-Y. Xing,
xingzanyang@sdu.edu.cn

Citation:
Wang, Y., Cao, Z., Xing, Z.-Y., Zhang, Q.-H., Jayachandran, P. T., Oksavik, K., et al. (2021). GPS scintillations and TEC variations in association with a polar cap arc. *Journal of Geophysical Research: Space Physics*, *126*, e2020JA028968. https://doi.org/10.1029/2020JA028968

Received 24 NOV 2020
Accepted 16 FEB 2021

Abstract A unique example of a polar cap arc producing clear amplitude and phase scintillations in GPS L-band signals is presented using observations from an all-sky imager and a GPS receiver and a digital ionosonde at Resolute Bay and the SuperDARN Inuvik radar. During the southward interplanetary magnetic field (IMF) condition, the polar cap arc moved quickly from the dusk-side to the midnight auroral oval at a speed of ~700 m/s, as revealed by all-sky 557.7 and 630.0 nm images. When it intersected the raypath of GPS signals, both amplitude and phase scintillations appeared, which is very different from previous results. Moreover, the scintillations were precisely determined through power spectral analysis. We propose that the strong total electron content (TEC) enhancement (~6 TECU) and flow shears in association with the polar cap arc under the southward IMF condition were creating the scintillations. It provides evidence for the existence of polar cap arc scintillations that may be harmful for satellite applications even through L-band signals.

Plain Language Summary Polar cap arcs are the large-scale aurora forms that stretch almost entirely across the polar cap and connect the dayside and night-side aurora oval. It is a common phenomenon in the polar region, often appearing as a single or multiple arcs. Previous observations suggested that polar cap arcs are producing clear total electron content (TEC) enhancement within different scales in association with particle precipitations under various energy levels. However, the corresponding scintillations especially the amplitude scintillation is still under controversy, which are requiring the precise evidence to decide the scintillation effects. We present here for the first time a case study of polar cap arc under the unique IMF condition to investigating the corresponding scintillation effects and also the TEC variations. The results reveal that the polar cap arc can produce both amplitude scintillation and phase scintillation clearly and significant TEC variations. It is showing us a new insight on the polar cap arcs, reminding us pay attention to the harmful effects on satellite/navigation applications.

1. Introduction

In the polar ionosphere, different types of large-scale irregularities are often generated, such as the polar cap patch (e.g., Crowley, 1996; Hosokawa, Kashimoto, 2009; Hosokawa, St-Maurice, et al., 2010; Hosokawa et al., 2019, Wang et al., 2020; Zhang et al., 2013), the tongue of ionization (e.g., Foster, 2005; Hosokawa, Tsugawa, et al., 2010), the polar cap arc (e.g., Hosokawa et al., 2011; Xing et al., 2018; Zhu et al., 1997), and so forth. From these large-scale irregularities, a great number of smaller-scale irregularities appear at their edges through multiple plasma instability processes, for example, the gradient-drift instability and/or flow shear instability (or Kelvin-Helmholtz instability) (e.g., Basu et al., 1998, 1990; Carlson, 2012; Moen et al., 2013; van der Meeren et al., 2014; Wang et al., 2016).

When a radio signal travels through these small-scale ionospheric irregularities, it is often degraded or even interrupted, which is widely known as the ionospheric scintillation. Previous studies concluded that the phase scintillation is generally caused by the irregularities at scales from hundreds of meters to several kilometers. While, the amplitude scintillation is usually generated by the irregularities at smaller scales from

hundreds of meters down to tens meters, which is confirmed from observations and simulations (e.g., Moen et al., 2013; van der Meeren et al., 2014, 2016; Wang et al., 2016, 2018).

At high latitudes, the effects of scintillations associated with a variety of ionospheric irregularities have been investigated in many studies (e.g., Jayachandran et al., 2017; Jin et al., 2014, 2015, 2016; Moen et al., 2013; Mushini et al., 2018; Oksavik et al., 2015; van der Meeren et al., 2014, 2015; Wang et al., 2016; and references therein). In this study, we are focusing on the polar cap arc, which is an aurora arc in the polar cap region that is primarily formed during northward interplanetary magnetic field (IMF) and under a quiet geomagnetic condition (e.g., Fear et al., 2014; Kullen, 2012; Xing et al., 2018; Zhu et al., 1997). Some polar cap arcs extend all the way across the polar cap, connecting the nightside and dayside aurora oval, which are usually called theta aurora or transpolar arcs (e.g., Frank et al., 1982). Meanwhile, most polar cap arcs often extend on shorter spatial scales, and likely emerge on the duskside or dawnside of the polar cap (Valladares et al., 1994; Shiokawa et al., 1996, 1997). The formation and dynamics of the polar cap arc have been debated for decades, and it still remains unclear whether it is driven by dayside or nightside reconnection processes (e.g., Kullen, 2012; Xing et al., 2018; Zhu et al., 1997). Previous works have identified that the polar cap arc is definitely corresponding to strong plasma flow shears and field-aligned currents (e.g., Fear et al., 2014; Herlingshaw et al., 2019; Milan et al., 2005; Moen et al., 2013; Xing et al., 2018; Zou et al., 2015). Based on multi-instrument observations and 3D MHD simulations, Zhang et al. (2020) recently proposed a mechanism for the formation of auroral arcs (including the polar cap arc) via field-aligned acceleration of electrons through the Knight's current-voltage process caused by the field aligned current (FAC) sheets that are generated by strong flow shears in the magnetosphere.

Consequently, the ionospheric irregularities of polar cap arcs might be a space weather concern, which are possibly structured by flow shears through the Kelvin-Helmholtz instability (Moen et al., 2013). Several studies have reported polar cap arcs producing scintillations for 250 MHz radio signals (e.g., Basu et al., 1990; Buchau et al., 1985). However, observations of scintillation for L-band signal (~1.2–1.6 GHz) in relation to the polar cap arc remains unknown due to the limited coverage of measurements in the central polar cap. Prikryl et al. (2015) mentioned that only moderate to strong phase scintillations were induced by the polar cap arc. However, these improved phase scintillations were probably attributed to the high-speed plasma flows according to Wang et al. (2018). On the contrary, van der Meeren et al. (2016) found that a polar cap arc in the night-side ionosphere produced very little scintillations (only weak phase scintillation), which was likely explained by the low background ionospheric density in the polar cap after a long period of northward IMF. Moreover, Jayachandran et al. (2012, 2017) presented a different type of Sun-aligned arcs detached near the poleward of dawnside auroral oval (with much smaller size in a couple of hundreds kms), which were clearly producing both total electron content (TEC) variations and scintillations. They gave a precursor on the possibility of polar cap arcs to induce amplitude and phase scintillations. However, for that event it was not yet possible to precisely separate the effects of Sun-aligned arcs from the auroral oval due to their small separation. Zhang et al. (2017) defined the polar cap hot patch and suggested it may associate with polar cap arcs and stronger scintillations. Furthermore, the positive relations of auroral emissions and phase scintillations have been statistically established, generally higher values of emission intensity correspond to stronger phase scintillation (Kinrade et al., 2013; Mushini et al., 2018). Additionally, Kintner et al. (2002) and Jayachandran et al. (2009) reported TEC variations due to an auroral arc, but there were no analysis on scintillations. Herlingshaw et al. (2019) presented a polar cap arc with an associated flow channel, but they did not focus on scintillation or TEC effects. Therefore, a comprehensive investigation into the dynamics of the polar cap arc and any association to scintillations still remains to be done.

Fortunately, the Resolute Bay station in the central polar cap provides a unique opportunity to investigate the evolution of both polar cap arcs and scintillation features, with combined observations from an all-sky imager, a GPS receiver, and the Super Dual Aurora Radar Network (SuperDARN) Inuvik radar.

2. Instruments

In this study, the all-sky imager of 557.7 nm and 630.0 nm wavelengths at Resolute Bay (74.75°N, 265.0°E in geographic coordinate; 82.9°N magnetic latitude) is used for visualizing the polar cap arc structures at a cadence of 2 min as a function of elevation and azimuth. Resolute Bay is one station of the Optical

Mesosphere Thermosphere Imagers (OMTIs) for network measurements of aurora and airglow (Hosokawa et al., 2009; Shiokawa et al., 1999). Moreover, the NovAtel GSV4004b GPS receiver is co-located with the all-sky imager, making raw data samples at 50 Hz. It is a part of the Canadian High Arctic Ionospheric Network (CHAIN) (Jayachandran et al., 2009). Based on the raw data from the GPS receiver, the amplitude scintillation index (S_4, normalised standard deviation of the signal amplitude over a specific interval) and the phase scintillation index (σ_φ, standard deviation of the signal phase during a certain period) were calculated using the wavelet detrended method at a 10 s cadence (e.g., Mushini et al., 2012). In order to lower the multipath effect, all data below 15° elevation were masked (e.g., Wang et al., 2016, 2018). Furthermore, the plasma flow data from the SuperDARN Inuvik radar were used to monitor the line-of-sight (LOS) motion of decameter-scale field-aligned plasma irregularities (Greenwald et al., 1995). In this study, the region of interest is fully covered by the SuperDARN Inuvik radar. Additionally, the solar wind and IMF data were obtained from the OMNI-2 website. These data are already time-shifted to the nose of the bow shock. Considering the solar wind propagation from the nose of the bow shock to the polar ionosphere, an additional time delay of 7 min was used according to the former results (e.g., Liou et al., 1998).

3. Observations

Figure 1 summarizes an interesting case of polar cap arcs during 06:00–08:00 UT on December 3, 2011. The period of interest in this study is shown by the black dashed frame (07:10–07:45 UT). Figures 1a–1c represent the IMF conditions and solar wind, consisting of the IMF Bx (blue), By (black), and Bz (red) components in Geocentric Solar Magnetic (GSM) coordinates (a); solar wind velocity (V_{SW}, black) and solar wind density (N_P, red; b); and dynamic pressure (P_{Dyn}; c). Figures 1d and 1e show the amplitude scintillation index (S_4) and phase scintillation index (σ_ϕ), respectively, which were computed from the 50 Hz raw data of the Resolute Bay GPS receiver at 10 s time resolution. During this period, all tracked GPS satellites were color coded according to the color bar on the right-hand side and then labeled by their GPS pseudo random noise code (PRN). Figures 1f and 1g present keograms of aurora emissions, respectively, which were extracted from the all-sky 630.0 nm (f) and 557.7 nm (g) images along the magnetic meridian line between elevation angles of 15° (magnetic north) and 165° (magnetic south) at Resolute Bay.

The IMF Bz (the red line in Figure 1a) is initially positive and then sharply changes to stable negative from ~06:45 UT. The IMF By component is negative the whole time, while IMF Bx changes from positive to negative (the black and blue lines in Figure 1a, respectively). The solar wind velocity, density, and dynamic pressure all dramatically decreased at around ~06:45 UT. Focusing on the framed region, the IMF Bz is constantly negative (around −6 nT), as well as the IMF By and IMF Bx components, together with the quiet solar wind conditions. Looking at the auroral keograms in Figures 1f and 1g (07:10–07:45 UT), a brightening narrow structure is rapidly drifting from top (magnetic north) to bottom (magnetic south) in both 630.0 and 557.7 nm emissions, which is typical for a polar cap arc (e.g., Hosokawa et al., 2011; Jayachandran et al., 2012). Simultaneously, the scintillations in Figures 1d and 1e become active. There was also another polar cap arc around ~06:45 UT (before the black dashed frame) in Figures 1f and 1g, which also had active scintillations. Below we investigate the relations of the polar cap arc and scintillations in further detail.

Figure 2 lists a sequence of images of aurora emissions observed by the all-sky imager in 557.7 nm (a–f; left) and 630.0 nm (g–l; right) as a function of elevation (greater than 15°) and azimuth during the period of 07:20–07:38 UT on December 3, 2011, as well as the magnitude of scintillations of amplitude (blue cross) and phase (red circle) according to the four levels indicated below the figure. Magnetic north is at the top, and magnetic west to the right. The white dashed vertical lines represent the magnetic meridian line along North-South direction across the zenith of all-sky images. The scintillations are precisely located along the LOS directions from the GPS satellites to the ground receiver. The color bar in the middle represents the intensity scale of auroral emissions in Rayleigh. From the 557.7 nm images to the left (Figures 2a–2f), a brightening band is generally stretching from northeast to southwest at the top right edge of Figure 2a, which is moving fast from northwest toward southeast across the Field-of-View with an average speed of ~700 m/s according to the images. With Resolute Bay in the central polar cap, this brightening band is thus a polar cap arc, which is appearing in the 630.0 nm images in a similar manner (Figures 2g–2l). The polar cap arc gradually increased in intensity during this period. When the polar cap arc moved across the GPS rays over Resolute Bay, it offered an opportunity to precisely compare the polar cap arc to variations

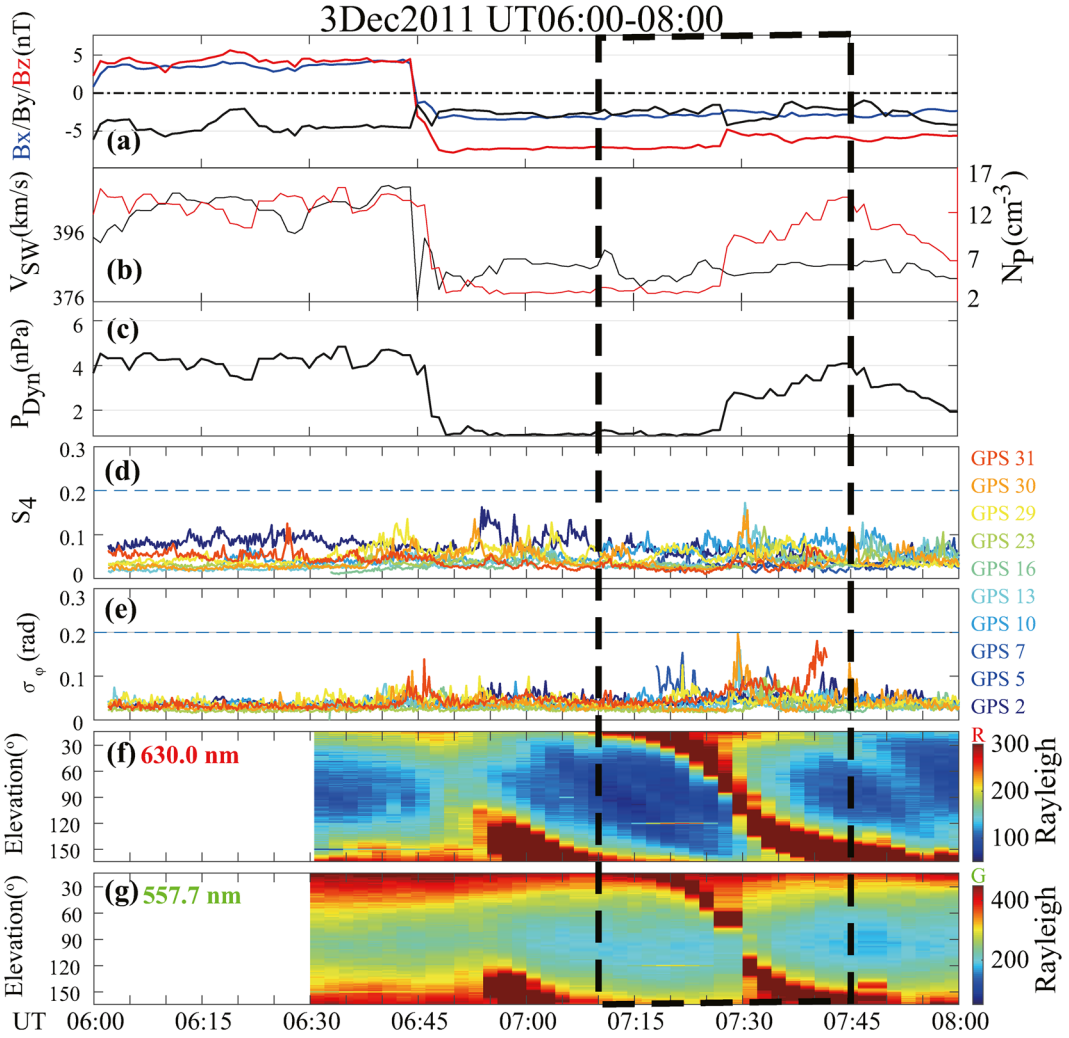

Figure 1. Panels (a)–(c) present the solar wind and interplanetary magnetic field (IMF) conditions, (a) IMF Bx (blue), By (black), and Bz (red) components, (b) solar wind speed (black) and density (red), and (c) solar wind dynamic pressure. The data were collected from the OMNI website and time-shifted 7 min to allow for propagation from the bow shock nose to the polar ionosphere. Panels (d) and (e) represent the amplitude and phase scintillation indices at 10 s cadence. Panels (f) and (g) show keograms of auroral emissions observed by the Resolute Bay all-sky imager along the magnetic meridian line between elevation from 15° (magnetic north) to 165° (magnetic south) at 630.0 and 557.7 nm, respectively, which were indicated by the white dashed vertical lines in Figure 2. The region of interest is highlighted by the black dashed frame from 07:10 to 07:45 UT, and the bright narrow band from top to bottom in Panels (f) and (g) is the polar cap arc.

in scintillations and TEC. Note that the speed of the polar cap arc (~700 m/s) was much greater than the motion of the GPS rays (<50 m/s) at the altitude of the auroral emission (~100–200 km).

To check the effects of the polar cap arc on scintillations and TEC variations, the GPS PRN13 and PRN30 in Figure 2 were chosen due to their central locations in the all-sky imager Field-of-View. Before 07:26 UT (Figures 2a and 2b), the GPS PRN13 and PRN30 were near zenith but far from the polar cap arc. At 07:26 UT (Figure 2c) the polar cap arc approached these two GPS rays from the northwest. At 07:30 UT (Figure 2d), GPS PRN13 and PRN30 were located at the trailing edge of the polar cap arc. At this moment, both phase and amplitude scintillations grew in strength. When the polar cap arc moved away from these two GPS rays, the scintillations quickly reduced (Figures 2e and 2f). It suggests that the polar cap arc may affect both amplitude and phase scintillations. There are several similar examples of GPS satellites showing a similar scintillation pattern. In Figure 2b, the scintillation of a GPS satellite to the northeast experiences the peak

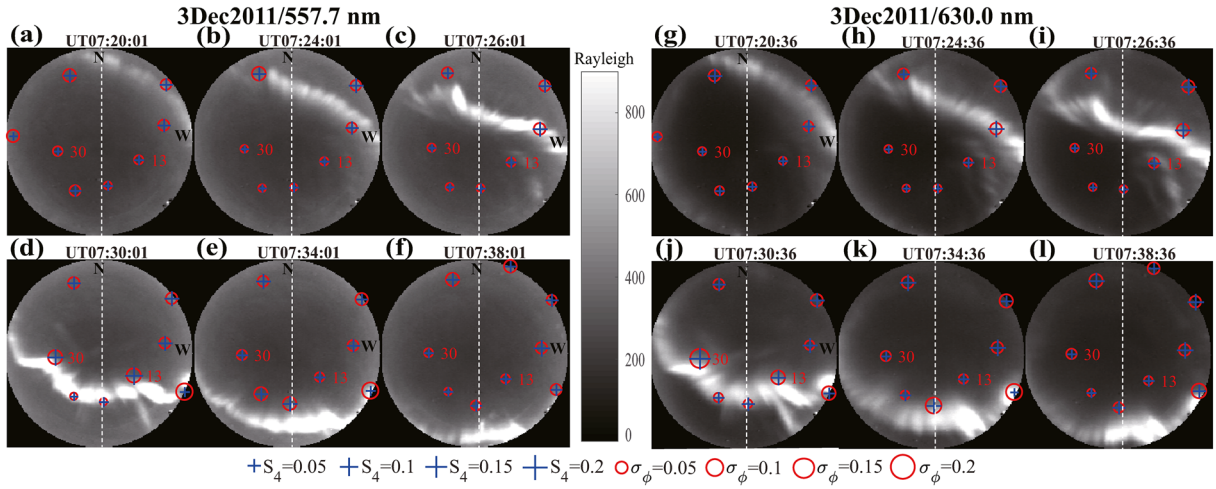

Figure 2. Auroral emissions in the all-sky imager Field of View from 07:20 to 07:38 UT on December 3, 2011. The 557.7 nm (left) and 630.0 nm (right) are shown, with the color bar in the middle representing the auroral intensity in Rayleigh. Magnetic north is at the top, and magnetic west is on the right. The white dashed vertical lines present the meridian line of the all-sky images along magnetic North-South direction across the zenith. The scintillations experienced by GPS rays are indicated by red circles (for phase scintillation) and blue crosses (for amplitude scintillation), with the corresponding scales at the bottom of the figure. GPS PRN13 and GPS PRN30 were selected as examples due to their good locations. A brightening auroral band structure extended from northeast to southwest and moved quickly toward southeast across the zenith of Resolute Bay in both sets of all-sky images.

when intersected by the polar cap arc, as well as the western satellite within the polar cap arc in Figure 2c. Moreover, there are three more GPS satellites in the south of Figures 2d–2f, clearly showing an enhancement of both amplitude and phase scintillations when intersected by the polar cap arc, followed by a quick return to background levels. Generally, the scintillations experienced by the satellites in the south are primarily greater than the ones in the north, which is consistent with the polar cap arc becoming brighter during the southward movement. Similarly, in the all-sky 630.0 nm images of Figures 2g–2l (to the right), a close match of polar cap arc and scintillations as mentioned above is showing up as expected. The gradually brightening polar cap arc is moving from northwest to southeast across zenith, which is stretching from northeast to southwest. When the polar cap arc intersects the rays of several GPS satellites, they experience various increases of both amplitude and phase scintillations, before quickly returning to background levels.

In order to clearly relate the polar cap arc, scintillations, and TEC variations, Figure 3 shows a time series of auroral intensities (a, b/f, g) and scintillations (c, d/h, i), as well as TEC (e/j) of GPS PRN13 (left column) and GPS PRN30 (right column). The two dashed gray vertical lines represent 07:29 UT. The auroral emissions were extracted from the all-sky imagers at around the GPS rays of the two satellites, green for 557.7 nm, red for 630.0 nm. Figures 3b and 3g (second row) present the temporal variations of auroral intensity calculated from Figures 3a and 3f (first row), respectively. In the first two rows (Figures 3a, 3b/3f, 3g), a significant enhancement of auroral intensities at 557.7 and 630.0 nm is clearly emerging at ~07:29 UT (dashed vertical lines), suggesting that the polar cap arc is moving across the GPS rays during this specific period. The surprising TEC enhancement (~6 TECU) is additional supportive evidence, as shown in Figures 3e and 3j (the last row). Note that these TECs are slant TECs with elevation angles of ~60° during the peak interval. In Figure 5, we have also checked the ionograms from CADI (Canadian Advanced Digital Ionosonde) at Resolute Bay, revealing that the polar cap arc is located at ~120 km (virtual height) under the elevation of 60° with peak frequency of ~8 MHz (e.g., Jayachandran et al., 2009). The peak electron density of the arc is $\sim 7.9 \times 10^{11}$ m^{-3}, which is a significant electron density. This indicates that the TEC variations associated with the polar cap arc are possibly related to the enhanced E region.

At the same time, amplitude and phase scintillations on GPS PRN13 and PRN30 are obviously peaking near 0.2 from the background (~0.05) (Figures 3c, 3d/3h, 3i, respectively). It may be noted that the main scintillation enhancement (during 07:29–07:33 UT) starts slightly after the immediate arrival of the arc (before 07:29 UT), compared to the scintillation before the passage of the arc. Figure 3 shows that when the polar cap arc is moving across the GPS rays, both amplitude and phase scintillations are produced,

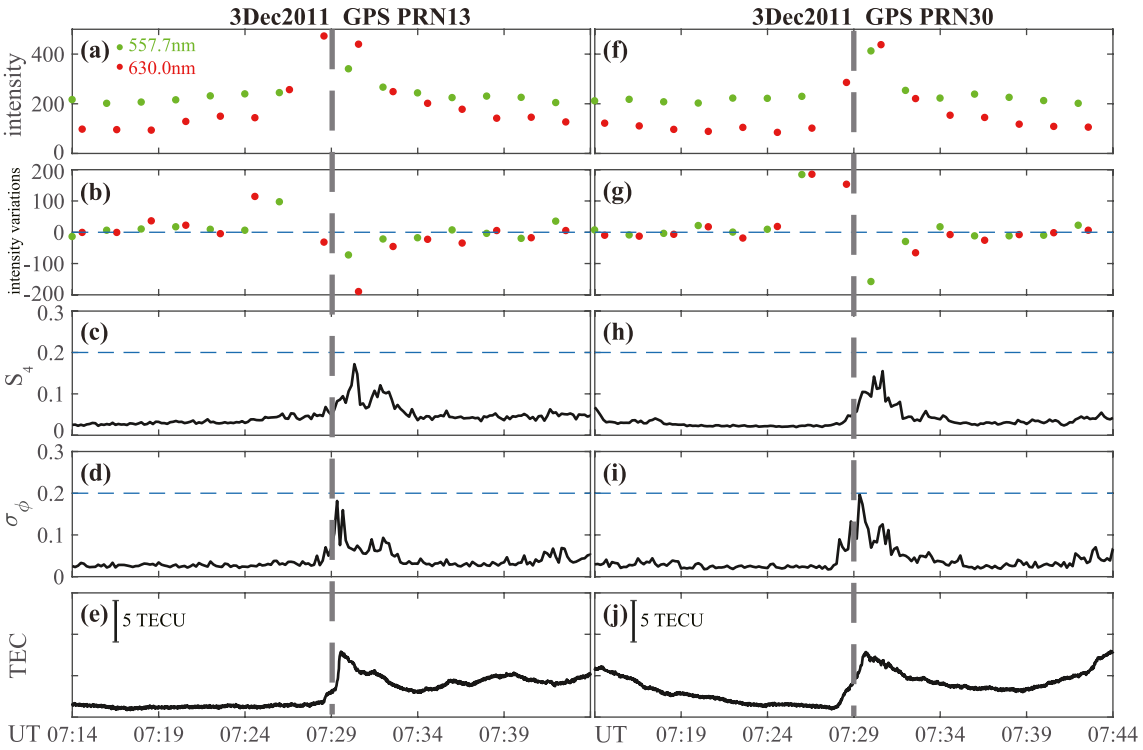

Figure 3. A time series of aurora emission intensities and GPS scintillations, as well as total electron content (TEC) variations from two selected satellites of GPS PRN13 (left) and PRN30 (right) at Resolute Bay from 07:14 to 07:44 UT on December 3, 2011. The gray dashed vertical line is highlighting the time of 07:29 UT. The first row shows the aurora intensities extracted from the all-sky imager at around the selected GPS satellite rays, red for 630.0 nm, blue for 557.7 nm; the second row present the temporal variations of aurora intensities; the third row represents the amplitude scintillation index (S_4); the fourth row shows the phase scintillation index (σ_ϕ); and the last row displays the TEC variations.

which documents that a polar cap arc can stimulate both amplitude and phase scintillations as well as TEC enhancements.

These scintillations are further checked in an analysis of power spectral density to exclude potential interference effects of refraction or multipath. Figure 4 presents the amplitude power spectra densities of GPS PRN13 (left) and PRN30 (right) before (first row, 07:26 UT), during (second row, 07:30 UT), and after (third row, 07:34 UT) the polar cap arc intersected these two GPS rays. Only in Figures 4b and 4e (second row, 07:30 UT), when the polar cap arc moved across the GPS rays, the power spectral densities follow a power-law structure within a frequency range from ~0.7 Hz (red dashed vertical lines) to ~7 Hz (gray dashed vertical lines), firmly identifying the characteristics of the scintillations produced by the polar cap arc. These power-law structures are identified by the blue solid slope. A linear fit results in slopes of −0.935 (Figure 4b) and −1.18 (Figure 4e), respectively. These are larger (weaker) than previous arc results (e.g., Jayachandran et al., 2017). In contrast, at the time of intersection (07:30 UT, Figures 4b and 4e) the power spectral densities are almost constant in the frequency range outside the highlighted region (shown by the blue dashed horizontal lines). Similarly, at the time before (first row, 07:26 UT) and after (third row, 07:34 UT), the power spectrum above 0.1 Hz is fairly flat (linearly fitted by blue dashed horizontal lines). These are completely different from the power-law structure as shown in Figures 4b and 4e (blue solid slope), which are considered as the background noise. Note that it is widely accepted that scintillation can be determined by the appearance of power-law structure in the analysis of power spectra of the affected signals (e.g., McCaffrey & Jayachandran, 2019). Therefore, we can confidently claim that the polar cap arc has produced both amplitude and phase scintillations simultaneously, though the power spectra of only the amplitude scintillation is shown here. The structure of phase power spectra usually shows a continued power-law shape, often starting from a much lower frequency (<0.1 Hz) than that of the amplitude (here starting from ~0.7 Hz, highlighted by the red dashed vertical lines). Regarding the different behavior of the amplitude and phase from one satellite signal in the power spectra analysis within the low frequency

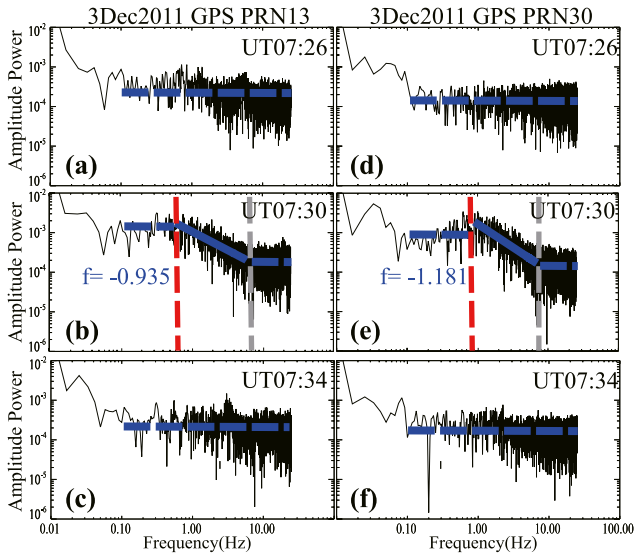

Figure 4. The power spectra analysis of the signal power of GPS PRN13 (left) and PRN30 (right), respectively, at specific times before (the first row), during (the second row), and after (the third row) the polar cap arc transit across the GPS rays. In the second row (07:30 UT), the power-law structures follow a slope in the frequency range between ~0.7 Hz (the red dashed vertical lines) and ~7 Hz (the gray dashed vertical lines), shown in the blue color. In the other two rows (07:26 UT and 07:34 UT) the power spectra are predominately flat above 0.1 Hz (shown with blue dashed horizontal lines).

region, it can be considered as the Fresnel filtering effect of the amplitude versus the phase (e.g., Carrano & Rino, 2016; Wang et al., 2018). In practice, we have checked the power spectral distributions of phase of these two GPS signals, which followed a simpler pattern and fitted to a power-law structure from a lower frequency (mostly between ~0.07 and ~3 Hz) compared to the amplitude.

4. Discussion

This section is divided into two parts to briefly discuss the dynamics of the polar cap arc, and then the possible mechanisms producing scintillations.

4.1. The Dynamics of Polar Cap Arc

Previous studies have shown that the polar cap arc usually occurs during northward IMF and a quiet geomagnetic state, and its evolution is often controlled by IMF (e.g., Berkey et al., 1976; Carter et al., 2017; Hosokawa et al., 2011; Kullen, 2012; Valladares et al., 1994; van der Meeren et al., 2016). According to the dynamic processes occurring at the dayside or nightside, the mechanisms of forming a polar cap arc have been roughly separated into two big groups: (1) polar cap arcs generated by the nightside dynamic processes in the magnetotail, and (2) polar cap arcs created by dayside dynamical processes (please see Xing et al., 2018; Zhang et al., 2020, and references therein).

For this event, after a sharp turning of IMF Bz from stable northward to stable southward, the polar cap arc initially formed on the dusk-side aurora oval and then migrated into the northern hemisphere central polar cap under a steady negative IMF By component (see Figure 1 for IMF conditions), which is consistent with previous results (Fear & Milan, 2012; Herlingshaw, et al., 2019; Zhu et al., 1997). After its formation, the polar cap arc moved fast toward the midnight auroral oval, which was recorded by the Resolute Bay all-sky imager in the midnight sector (see Figure 2). During the period of southward IMF, the polar cap arc gradually brightened, likely due to increased particle precipitation from magnetosphere-ionosphere coupling processes, that were possibly triggered by nightside magnetotail reconnection, which will be discussed in detail in Section 4.2. During the period of interest, the AU/AL indices gradually increased from ~0 to ~200 nT (not shown here), likely in response to nightside magnetotail reconnection.

4.2. Scintillation From the Polar Cap Arc

In our case, the polar cap arc is quickly intersecting the GPS ray paths, clearly enhancing both amplitude and phase scintillations. The level of amplitude and phase scintillations is almost up to 0.2 from the background noise level (~0.05). Before and after, the scintillations are subdued.

The corresponding plasma irregularities in the polar cap arc can be inferred from the enhanced scintillations, which may be formed by the combined effects of particle precipitation, flow shears, and electron density gradient instabilities associated with the polar cap arc. After a southward turning of the IMF, the intensity of the moving polar cap arc is gradually enhanced (e.g., Figures 2a–2f), which likely corresponds to particle precipitation from the magnetosphere to the ionosphere possibly due to nightside magnetotail reconnection. Here, the steady southward IMF condition of the polar cap arc is peculiar, which is fundamentally different from traditional studies (e.g., Jayachandran et al., 2017; van der Meeren et al., 2016). This peculiar IMF condition likely prefers to trigger dayside/nightside magnetic reconnection. Note that the southward IMF condition prefers to trigger dayside magnetopause reconnection (e.g., Lockwood and Carlson, 1992), usually accompanied by enhanced rates of nightside magnetotail reconnection (e.g., Zhang et al., 2015). These processes are not only enhancing the background density of the polar cap, but also

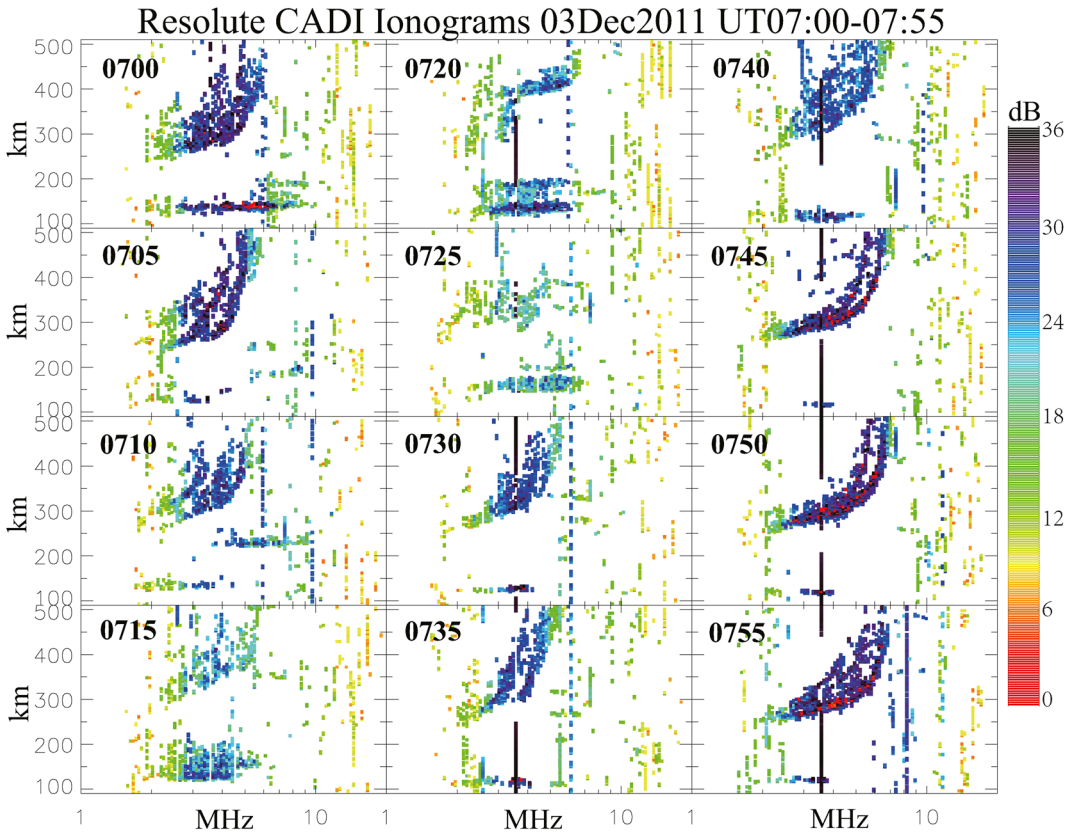

Figure 5. Sequence of 5 min interval ionograms for 0700–0755 UT on December 3, 2011 provided by the Canadian Advanced Digital Ionosonde (CADI) at Resolute, Canada.

inducing more particle precipitation, which is favorable for generation of plasma irregularities and production of scintillation. However, the specific relation of the polar cap arc to magnetic reconnection is beyond the scope of this study. Hence, it is concluded that the polar cap arc is not only enhanced in plasma density but also likely ionized by the injected particles associated with the southward IMF conditions.

Considering the general anti-sunward convection in the polar cap during a steady southward IMF condition (provided by SuperDARN observations, not shown here) and also the polar cap arc (Figures 2 and 6), the significant TEC enhancement of polar cap arc (Figure 3) prefers to create scintillation-related small-scale plasma irregularities on the trailing edges through the gradient-drift instability (e.g., Hosokawa et al., 2016). The density gradient effect on the trailing edge of the polar cap arc is consistent with the results that the scintillation activities appeared slightly after the intersection time of the GPS rays (Figure 3).

Figure 6 presents further evidence based on auroral images at 630.0 nm and observations from the SuperDARN Inuvik radar. There are two color bars on right-hand side; the left one is for the SuperDARN velocity data (blue color toward the radar, and red color away from the radar), and the right one is for the auroral intensity of the 630.0 nm all-sky imager. The north is up and the west is left. Figures 6a–6f present a sequence of 630.0 nm aurora emissions superimposed on top of the MLat (magnetic latitude)-MLT (magnetic local time) grid, using an assumed emission altitude of 230 km. Figures 6g–6l present the LOS velocity from the SuperDARN Inuvik radar, corresponding to the times of the all-sky images. The black contours in Figures 6g–6l outline the boundaries of the polar cap arc as shown in Figures 6a–6f. In the SuperDARN radar observations (Figures 6h–6m), there is good backscatter near the polar cap arc (the black contour), strongly suggesting the presence of decameter-scale plasma irregularities (e.g., Greenwald et al., 1995; van der Meeren et al., 2016; Wang et al., 2020), which are likely related to scintillations. It is worth noting that the data gap in the velocity observations on the right-hand side of the arc contour is likely due to the observation altitude of the SuperDARN Inuvik radar being higher than the altitude where the arc or F layer irregularities

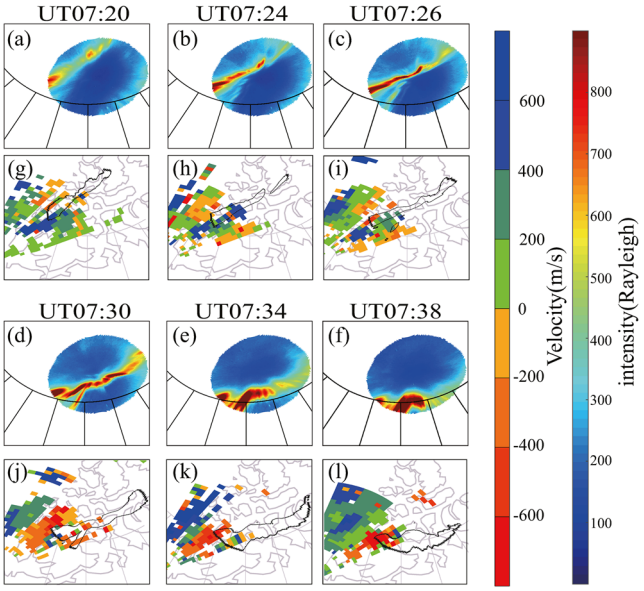

Figure 6. Examples of auroral emissions (a–f) from all-sky 630.0 nm images in comparison with the corresponding Field-of-View velocities of the SuperDARN Inuvik radar (g–l) from 07:20 to 07:38 UT on December 3, 2011. There are two color bars at the right-hand side; the left one is for the velocity (blue for toward radar, red for away from radar), and the right one is for the auroral emission measured in Rayleigh. The north is up; the west is left. The black solid contours in panels (g)–(l) outline the corresponding polar cap arc from panels (a)–(f), respectively.

often show up. Furthermore, the plasma flow shears generally occurred on the northwest side of the polar cap arc, especially after 07:24 UT (Figures 6h–6l), which is consistent with previous studies (e.g., Herlingshaw et al., 2019), suggesting generation of plasma irregularities and scintillations through flow-shear instabilities (Zhang et al., 2017, 2020). The flow shear enhancement on the northwest side of the polar cap arc is consistent with the fact that the scintillation enhancement occurs mainly through the passage of the arc, as shown in Figure 3.

5. Conclusions

In this study, a case study of a polar cap arc associated with enhanced amplitude and phase scintillations and TEC variations is presented by using joint-observations of the all-sky imager and GPS receiver and CADI at the Resolute Bay station, as well as the SuperDARN Inuvik radar. After a sudden change of IMF Bz from stable northward to stable southward, the polar cap arc moved quickly from the duskside toward the midnight auroral oval across the zenith of Resolute Bay at an average speed of ~700 m/s, which was recorded in both 557.7 and 630.0 nm all-sky images. When the polar cap arc intersected the GPS rays, significant enhancements of both amplitude and phase scintillations were observed by the GPS receiver, in addition to TEC enhancements.

Referring to the unique long duration southward IMF condition of this polar cap arc, these TEC variations and scintillations are likely explained by magnetic reconnections associated with the polar cap arc. The scintillation-related plasma irregularities could be produced by TEC density gradients due to enhanced particle precipitation from magnetosphere-ionosphere coupling processes and plasma flow shears possibly associated with nightside magnetotail reconnection. The magnetic field geometry linked to the southward IMF polar cap arc is unknown. More events will have to be studied to further establish the characteristics of polar cap arcs that have severe impact on scintillations and TEC enhancements.

Data Availability Statement

The authors sincerely appreciate the Physics department of University of New Brunswick for establishing and running CHAIN and providing the GPS receiver CADI data (http://chain.physics.unb.ca/chain/). They greatly thank Nagoya University for developing the OMTI and sharing the all-sky imager data (http://stdb2.isee.nagoya-u.ac.jp/omti/). They also acknowledge Virginia Tech. for providing SuperDARN radar data through their website (http://vt.superdarn.org/), and the NASA OmniWeb for providing the solar wind and IMF data (http://omniweb.gsfc.nasa.gov/html/sc_merge_data1.html).

Acknowledgments
This work was supported by the National Natural Science Foundation of China (grant No. 41604139, 41874170, and 41831072), China Postdoctoral Science Foundation funded project (2020M682163), and the National Key Laboratory of Electromagnetic Environment of China (6142403180103, and 6142403180102). K.Shiokawa is supported by JSPS KAKENHI (25247080, and 16H06286). K.Oksavik is supported by the Research Council of Norway under the contract 223252.

References

Basu, S., Basu, S., MacKenzie, E., Coley, W. R., Sharber, J. R., Hoegy, W. R. (1990). Plasma structuring by the gradient drift instability at high latitudes and comparison with velocity shear driven processes. *Journal of Geophysical Research*, *95*, 7799–7818. https://doi.org/10.1029/JA095iA06p07799

Basu, S., Weber, E. J., Bullett, T. W., Keskinen, M. J., MacKenzie, E., Doherty, P., et al. (1998). Characteristics of plasma structuring in the cusp/cleft region at Svalbard. *Radio Science*, *33*, 1885–1899. https://doi.org/10.1029/98RS01597

Berkey, T., Cogger, L. L., Ismail, S., & Kamide, Y. (1976). Evidence for a correlation between Sun-aligned arcs and the interplanetary magnetic field direction. *Geophysical Research Letters*, *3*, 145–147. https://doi.org/10.1029/GL003i003p00145

Buchau, J., Weber, E. J., Anderson, D. N., Carlson, H. C., Jr, Moore, J. G., Reinisch, B. W., & Livingstone, R. C. (1985). Ionospheric structures in the polar cap: Their origin and relation to 250-MHz scintillation. *Radio Science*, *20*, 325. http://doi.org/10.1029/RS020i003p00325

Carlson, H. C. (2012). Sharpening our thinking about polar cap ionospheric patch morphology, research, and mitigation techniques. *Radio Science*, *47*, RS0L21. https://doi.org/10.1029/2011RS004946

Carrano, C. S., & Rino, C. L. (2016). A theory of scintillation for two-component power law irregularity spectra: Overview and numerical results. *Radio Science*, *51*, 789–813. https://doi.org/10.1002/2015RS005903

Carter, J. A., Milan, S. E., Fear, R. C., Walach, M.-T., Harrison, Z. A., Paxton, L. J., & Hubert, B. (2017). Transpolar arcs observed simultaneously in both hemispheres. *Journal of Geophysical Research: Space Physics*, *122*, 6107–6120. https://doi.org/10.1002/2016JA023830

Crowley, G. (1996). Critical review of ionospheric patches and blobs. In W. R. Stone (Ed.), *Review of radio science 1992-1996* (pp. 619–648). Oxford University Press.

Fear, R. C., & Milan, S. E. (2012). The IMF dependence of the local time of transpolar arcs: Implications for formation mechanism. *Journal of Geophysical Research*, *117*, A03213. https://doi.org/10.1029/2011JA017209

Fear, R. C., Milan, S. E., Maggiolo, R., Fazakerley, A. N., Dandouras, I., & Mende, S. B. (2014). Direct observation of closed magnetic flux trapped in the high-latitude magnetosphere. *Science*, *346*, 1506–1510. https://doi.org/10.1126/science.1257377

Foster, J. C., Coster, A. J., Erickson, P. J., Holt, J. M., Lind, F. D., Rideout, W., et al. (2005). Multiradar observations of the polar tongue of ionization. *Journal of Geophysical Research*, *110*, A09S31. https://doi.org/10.1029/2004JA010928

Frank, L. A., Craven, J. D., Burch, J. L., & Winningham, J. D. (1982). Polar views of the Earth's aurora with dynamics explorer. *Geophysical Research Letters*, *9*, 1001–1004. https://doi.org/10.1029/GL009i009p01001

Greenwald, R. A., Bristow, W. A., Sofko, G. J., Senior, C., Cerisier, J.-C., Szabo, A. (1995). Super dual aurora radar network radar imaging of dayside high-latitude convection under northward interplanetary magnetic field: Toward resolving the distorted two-cell versus multicell controversy. *Journal of Geophysical Research*, *100*, A10. https://doi.org/10.1029/95JA01215

Herlingshaw, K., Baddeley, L. J., Oksavik, K., Lorentzen, D. A., & Bland, E. C. (2019). A study of automatically detected flow channels in the polar cap ionosphere. *Journal of Geophysical Research: Space Physics*, *124*. https://doi.org/10.1029/2019JA026916

Hosokawa, K., Kashimoto, T., Suzuki, S., Shiokawa, K., Otsuka, Y., & Ogawa, T. (2009a). Motion of polar cap patches: A statistical study with all-sky airglow imager at Resolute Bay, Canada. *Journal of Geophysical Research*, *114*, A04318. https:/doi.org/10.1029/2008JA014020

Hosokawa, K., Moen, J. I., Shiokawa, K., & Otsuka, Y. (2011). Motion of polar cap arcs. *Journal of Geophysical Research*, *116*, A01305. https://doi.org/10.1029/2010JA015906

Hosokawa, K., Shiokawa, K., Otsuka, Y., Ogawa, T., St-Maurice, J. P., Sofko, G. J., & Andre, D. A. (2009b). Relationship between polar cap patches and field-aligned irregularities as observed with an all-sky airglow imager at Resolute Bay and the PolarDARN radar at Rankin inlet. *Journal of Geophysical Research*, *114*. https://doi.org/10.1029/2008ja013707

Hosokawa, K., St-Maurice, J.-P., Sofko, G. J., Shiokawa, K., Otsuka, Y., & Ogawa, T. (2010a). Reorganization of polar cap patches through shears in the background plasma convection. *Journal of Geophysical Research*, *115*, A01303. https://doi.org/10.1029/2009JA014599

Hosokawa, K., Taguchi, S., & Ogawa, Y. (2016). Edge of polar cap patches. *Journal of Geophysical Research: Space Physics*, *121*. https://doi.org/10.1002/2015JA021960

Hosokawa, K., Tsugawa, T., Shiokawa, K., Otsuka, Y., Nishitani, N., Ogawa, T., & Hairston, M. R. (2010b). Dynamic temporal evolution of polar cap tongue of ionization during magnetic storm. *Journal of Geophysical Research*, *115*, A12333. https://doi.org/10.1029/2010JA015848

Hosokawa, K., Zou, Y., & Nishimura, Y. (2019). Airglow patches in the polar cap region: A review. *Space Science Reviews*, *215*, 8. https://doi.org/10.1007/s11214-019-0616-8

Jayachandran, P. T., Hamza, A. M., Hosokawa, K., Mezaoui, H., & Shiokawa, K. (2017). GPS amplitude and phase scintillation associated with polar cap aurora forms. *Journal of Atmospheric and Terrestrial Physics*, *164*, 185–191. http://dx.doi.org/10.1016/j.jastp.2017.08.030

Jayachandran, P. T., Hosokawa, K., MacDougall, J. W., Mushini, S., Langley, R. B., & Shiokawa, K. (2009b). GPS total electron content variations associated with a polar cap arc. *Journal of Geophysical Research*, *114*, A12304. https://doi.org/10.1029/2009JA014916

Jayachandran, P. T., Hosokawa, K., Shiokawa, K., Otsuka, Y., Watson, C., Mushini, S. C., et al. (2012). GPS total electron content variations associated with poleward moving Sun-aligned arcs. *Journal of Geophysical Research*, *117*, A05310. https://doi.org/10.1029/2011JA017423

Jayachandran, P. T., Langley, R. B., MacDougall, J. W., Mushini, S. C., Pokhotelov, D., Hamza, A. M., et al. (2009). Canadian High Arctic Ionospheric Network (CHAIN). *Radio Science*, *44*, RS0A03. https://doi.org/10.1029/2008RS0040046

Jin, Y., Moen, J., & Miloch, W. J. (2014). GPS scintillation effects associated with polar cap patches and substorm aurora activity: Direct comparison. *Journal of Space Weather and Space Climate*, *4*, A23. https://doi.org/10.1051/SWSC/2014019

Jin, Y., Moen, J., & Miloch, W. J. (2015). On the colocation of the cusp aurora and the GPS phase scintillation: A statistical study. *Journal of Geophysical Research: Space Physics*, *120*, 9176–9191. https://doi.org/10.1002/2015JA021449

Jin, Y., Moen, J. I., Miloch, W. J., Clausen, L. B. N., & Oksavik, K. (2016). Statistical study of the GNSS phase scintillation associated with two types of aurora blobs. *Journal of Atmospheric and Solar-Terrestrial Physics*, *121*, 4679–4697. https://doi.org/10.1002/2016JA022613

Kinrade, J., Mitchell, C. N., Smith, N. D., Ebihara, Y., Weatherwax, A. T., & Bust, G. S. (2013). GPS phase scintillation associated with optical auroral emissions: First statistical results from the geographic South Pole. *Journal of Geophysical Research*, *118*, 2490–2502. https://doi.org/10.1002/jgra.50214

Kintner, P. M., Kil, H., Deehr, C., & Schuck, P. (2002). Simultaneous total electron content and all-sky camera measurements of an auroral arc. *Journal of Geophysical Research*, *107*(A7), 1127. https://doi.org/10.1029/2001JA000110

Kullen, A. (2012). Transpolar arcs: Summary and recent results. In A. Keiling, E. Donovan, F. Bagenal, & T. Karlsson (Eds.), Geophysical monograph 197 (pp. 69–80). American Geophysical Union.

Liou, K., Newell, P. T., Meng, C. I., Brittnacher, M., Parks, G.(1998). Characteristics of the solar wind controlled auroral emissions. *Journal of Geophysical Research - D: Atmospheres*, *103*, 17543–17558. https://doi.org/10.1029/98JA01388

Lockwood, M., & Carlson, H. C. (1992). Production of polar cap electron density patches by transient magnetopause reconnection. *Geophysical Research Letters*, *19*, 1731–1734. https://doi.org/10.1029/92GL01993

McCaffrey, A. M., & Jayachandran, P. T. (2019). Determination of the refractive contribution to GPS phase "scintillation". *Journal of Geophysical Research: Space Physics*, *124*, 1454–1469. http://doi.org/10.1029/2018JA025759

Milan, S. E., Hubert, B., & Grocott, A. (2005). Formation and motion of a transpolar arc in response todayside and nightside reconnection. *Journal of Geophysical Research*, *110*. https://doi.org/10.1029/2004JA010835

Moen, J., Oksavik, K., Alfonsi, L., Daabakk, Y., Romano, V., & Luca Spogli, L. (2013). Space weather challenges of the polar cap ionosphere. *Journal of Space Weather and Space Climate*, *3*, A02. https://doi.org/10.1051/SWSC/2013025

Mushini, S. C., Jayachandran, P. T., Langley, R. B., MacDougall, J. W., & Pokhotelov, D. (2012). Improved amplitude- and phase-scintillation indices derived from wavelet detrended high-latitude GPS data. *GPS Solutions*, *16*, 363–373. https://doi.org/10.1007/s10291-011-0238-4

Mushini, S. C., Skone, S., Spanswick, E., Donovan, E., & Najmafshar, M. (2018). Proxy index derived from All Sky Imagers for space weather impact on GPS. *Space Weather*, *16*, 838–848. https://doi.org/10.1029/2018SW001919

Oksavik, K., van der Meeren, C., Lorentzen, D. A., Baddeley, L. J., & Moen, J. (2015). Scintillation and loss of signal lock from poleward moving aurora forms in the cusp ionosphere. *Journal of Geophysical Research: Space Physics*, *120*, 9161–9175. https://doi.org/10.1002/2015JA021528

Prikryl, P., Jayachandran, P. T., Chadwick, R., & Kelly, T. D. (2015). Climatology of GPS phase scintillation at northern high latitudes for the period from 2008 to 2013. *Annales Geophysicae*, *33*, 531–545. https://doi.org/10.5194/angeo-33-531-2015

Shiokawa, K., Katoh, Y., Satoh, M., Ejiri, M. K., Ogawa, T., Nakamura, T., et al. (1999). Development of optical mesosphere thermosphere imagers (OMTI). *Earth Planets and Space*, *51*, 887–897. 10.1186/BF03353247

Shiokawa, K., Ogino, T., Hayashi, K., & McEwen, D. J. (1997). Quasi-periodic poleward motions of morningside Sun-aligned arcs: A multievent study. *Journal of Geophysical Research*, *102*. 24325–24332. https://doi.org/10.1029/97JA02383

Shiokawa, K., Yumoto, K., Nishitani, N., Hayashi, K., Oguti, T., McEwen, D. J., et al. (1996). Quasi-periodic poleward motions of sun-aligned auroral arcs in the high-latitude morning sector: A case study. *Journal of Geophysical Research*, *101*, 19789–19800. https://doi.org/10.1029/96JA01202

Valladares, C. E., Carlson, H. C., & Fukui, K. (1994). Interplanetary magnetic field dependency of stable sun-aligned polar cap arcs. *Journal of Geophysical Research*, *99*, 6247–6272. https://doi.org/10.1029/93JA03255

van der Meeren, C., Oksavik, K., Lorentzen, D., Moen, J. I., & Romano, V. (2014). GPS scintillation and irregularities at the front of an ionization tongue in the nightside polar ionosphere. *Journal of Geophysical Research: Space Physics*, *119*, 8624–8636. https://doi.org/10.1002/2014JA020114

van der Meeren, C., Oksavik, K., Lorentzen, D. A., Paxton, L. J., & Clausen, L. B. N. (2016). Scintillation and irregularities from the nightside part of a sun-aligned polar cap arc. *Journal of Geophysical Research: Space Physics*, *121*, 5723–5736. https://doi.org/10.1002/2016ja022708

van der Meeren, C., Oksavik, K., Lorentzen, D. A., Rietveld, M. T., & Clausen, L. B. N. (2015). Severe and localized GNSS scintillation at the poleward edge of the nightside aurora oval during intense substorm aurora. *Journal of Geophysical Research: Space Physics*, *120*, 10607–10621. https://doi.org/10.1002/2015ja021819

Wang, Y., Zhang, Q.-H., Jayachandran, P. T., Lockwood, M., Zhang, S.-R., Moen, J., et al. (2016). A comparison between large-scale irregularities and scintillations in the polar ionosphere. *Geophysical Research Letters*, *43*, 4790–4798. https://doi.org/10.1002/2016GL069230

Wang, Y., Zhang, Q.-H., Jayachandran, P. T., Moen, J., Xing, Z.-Y., Chadwick, R., et al. (2018). Experimental evidence on the dependence of the standard GPS phase scintillation index on the ionospheric plasma drift around noon sector of the polar ionosphere. *Journal of Geophysical Research: Space Physics*, *123*, 2370–2378. https://doi.org/10.1002/2017JA024805

Wang, Y., Zhang, Q.-H., Ma, Y.-Z., Jayachandran, P. T., Xing, Z.-Y., Balan, N., & Zhang, S.-R. (2020). Polar ionospheric large-scale structures and dynamics revealed by TEC keogram extracted from TEC maps. *Journal of Geophysical Research: Space Physics*, *125*, e2019JA027020. https://doi.org/10.1029/2019JA027020

Xing, Z., Zhang, Q., Han, D., Zhang, Y., Sato, N., Zhang, S., et al. (2018). Conjugate observations of the evolution of polar cap arcs in both hemispheres. *Journal of Geophysical Research: Space Physics*, *123*. https://doi.org/10.1002/2017JA024272

Zhang, Q.-H., Lockwood, M., Foster, J. C., Zhang, S.-R., Zhang, B.-C., McCrea, I. W., et al. (2015). Direct observations of the full Dungey convection cycle in the polar ionosphere for southward interplanetary magnetic field conditions. *Journal of Geophysical Research: Space Physics*, *120*, 4519–4530. https://doi.org/10.1002/2015JA021172

Zhang, Q.-H., Ma, Y.-Z., Jayachandran, P. T., Moen, J., Lockwood, M., Zhang, Y.-L., et al. (2017). Polar cap hot patches: Enhanced density structures different from the classical patches in the ionosphere. *Geophysical Research Letters*, *44*, 8159–8167. https://doi.org/10.1002/2017GL073439

Zhang, Q.-H., Zhang, B. C., Lockwood, M., Hu, H. Q., Ruohoniemi, J. M., et al. (2013). Direct observations of the evolution of polar cap ionization patches. *Science*, *339*, 1597–1600. https://doi.org/10.1126/science.1231487

Zhang, Q. -H., Zhang, Y.-L., Wang, C., Lockwood, M., Yang, H.-G., Tang, B.-B., et al. (2020). Multiple transpolar auroral arcs reveal insight about coupling processes in the Earth's magnetotail. *Proceedings of the National Academy of Sciences of the United States of America*, *117*, 16193–16198. https://doi.org/10.1073/pnas.2000614117

Zhu, L., Schunk, R. W., & Sojka, J. J. (1997). Polar cap arcs: a review. *Journal of Atmospheric and Solar-Terrestrial Physics*, *59*, 1087–1126. https://doi.org/10.1016/S1364-6826(96)00113-7

Zou, Y., Nishimura, Y., Lyons, L. R., Donovan, E. F., Shiokawa, K., Ruohoniemi, J. M., et al. (2015). Polar cap precursor of nightside auroral oval intensifications using polar cap arcs. *Journal of Geophysical Research: Space Physics*, *120*, 10698–10711. https://doi.org/10.1002/2015JA021816